

Upper Atmosphere and Extra-Planetary Rarefied Flows

MAE 5010 Microflows

Charles R. O'Neill

14 April 2005

1 Introduction

This paper's objective is to survey the Earth's upper atmosphere, including unique meteorological *phenomena* and rarefied aerodynamics. The upper atmosphere's fluid and electrical properties couple in interesting and unexpected ways.

The first section surveys the atmosphere. A meteorology section discusses specific upper altitude *phenomena*. The final section discusses rarefied aerodynamics.

2 Atmospheric Survey

This section's objective is to survey the Earth's atmosphere with emphasis on the upper atmosphere. Dowling¹ states:

Earth's atmosphere receives more energy per unit area than any other planetary atmosphere (including Venus), and yet has the weakest winds in the Solar System. This is an indication that the terrestrial problem is complicated... In fact,

Earth has the most unpredictable weather in the solar system, and that is saying something when one considers that the Sun, eight of the nine planets, and three of sixty-one moons have atmospheres.

Atmospheric models are needed for reference and design. AIAA's *Guide to Reference and Standard Atmospheric Models*² provides an evaluation and comparison of the many modern atmospheric models. For this paper, the *U.S. Standard Atmosphere, 1976*³ is used.

Figure 1 gives temperature versus altitude with the atmospheric layers superimposed. *Easily charged electrons in the rarefied thermosphere, allows for vastly varying atmospheric properties depending on the sun's electromagnetic activity. The existence and location of upper atmospheric phenomena depends on these varying atmospheric properties.*

The atmosphere's bottom layer up to about 10 km is the troposphere⁴, which is certainly not rarefied. Moisture convection and surface geometry dominates the tropo-

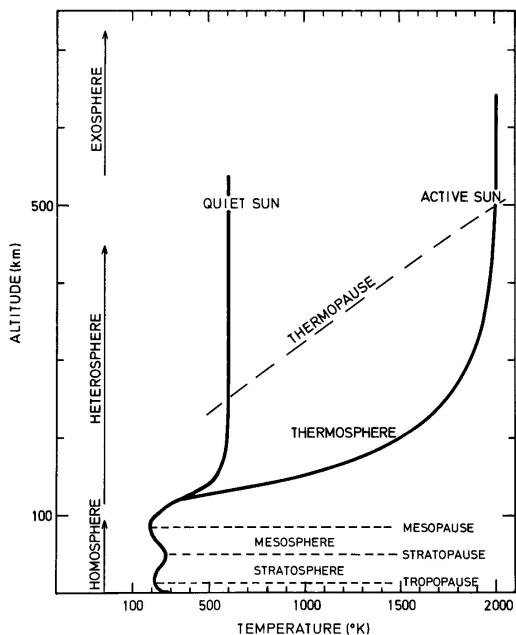


Figure 1: Atmospheric Temperatures and Layers from Sea-Level Upwards⁴

sphere's fluid flow. The linearized governing equation for vertical motion is⁵:

$$\frac{d^2z}{dt^2} = -\frac{g}{T}(\Gamma - \gamma)z$$

where Γ and γ are the local and environmental lapse rates¹, which are directly correlated with moisture content. Convective clouds form when temperature differences cause unstable rising air.

Figure 2 shows the mean free path λ versus altitude from sea-level to 1000 kilometers. λ increases as altitude increases. The initial slope below 100 km is approximately one order of magnitude increase per 15 km. The

¹vertical temperature gradient, dT/dz

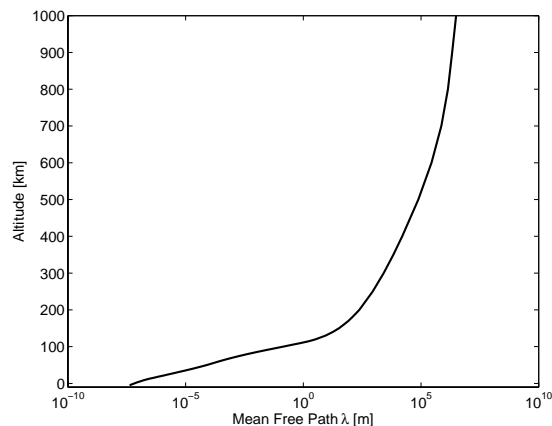


Figure 2: Atmospheric Mean Free Path Model, λ , as estimated from the 1976 Standard³

λ curve is comprised of two different behaviors with the cut-off at approximately 150 km. Notice that λ appears vary as a power law near the earth's surface. The mean free path at 100 km is approximately 1 m, which indicates that rarefied flow for man-made objects occurs at and above 100 km.²

Figure 3 shows density as a function of altitude. Density decreases as altitude increases. The initial slope below 100 km is approximately one order of magnitude decrease per 15 km. As with λ , density behavior changes at approximately 150 km. Density decreases some 8 orders of magnitude between sea-level and 100 km.

Electromagnetics become increasingly important as altitude increases. Electron number density versus altitude is given in Figure 4. Notice that above about 100 km, dis-

²Above 100 km is typically considered 'space'

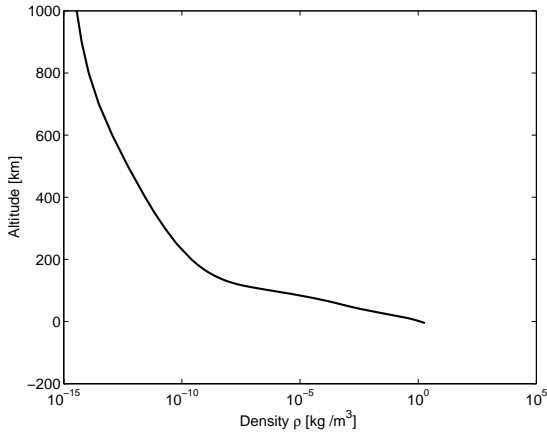


Figure 3: Atmospheric Density, ρ , as estimated from the 1976 Standard³

sociated electrons dominate the fluid. The sun easily ionizes these free electrons.

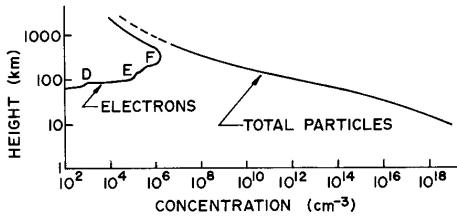


Figure 4: Electron/Total Number Density⁴

The earth's magnetic field creates the magnetosphere. Figure 5 shows a typical cross section cut centered on the earth. Significant electromagnetic and rarefied fluid coupling occurs in this region.⁶ Notice that the earth creates a solar wind shock.

3 Meteorology

This section's objective is to survey meteorological *phenomena* occurring in the upper

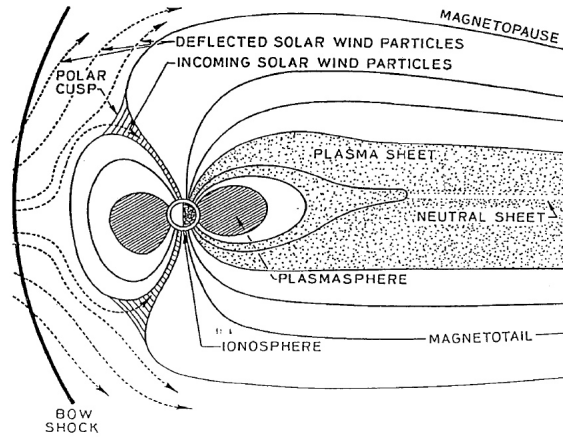


Figure 5: Magnetosphere⁶

atmosphere. *These phenomena are not isolated from the rarefied gas; the phenomena are the result of a physical process occurring in the gas. For the visible phenomena, the illumination typically occurs from molecular excitation and chemical storage.* Emphasis is placed on *phenomena* which only occur in a rarefied atmosphere. Interestingly, new *phenomena* are still being discovered.

3.1 Airglow

Airglow is a weak day and night illumination resulting from electron excitation in the upper atmosphere on the order of 100 km⁷. At this altitude, the rarefied gases allow for long time constants and chemical energy storage³. Smith⁸ found gravity waves influencing airglow at 100 km.

Ratcliffe says,⁷

The nightglow is extremely feeble, the illumination it gives to the

ground being of the same order as that from a candle at a height of 100 meters.

Figure 6 shows “[the] earth as seen from the moon in far-ultraviolet (125–160 nm) light. The light includes radiation from atomic oxygen and molecular nitrogen.³”

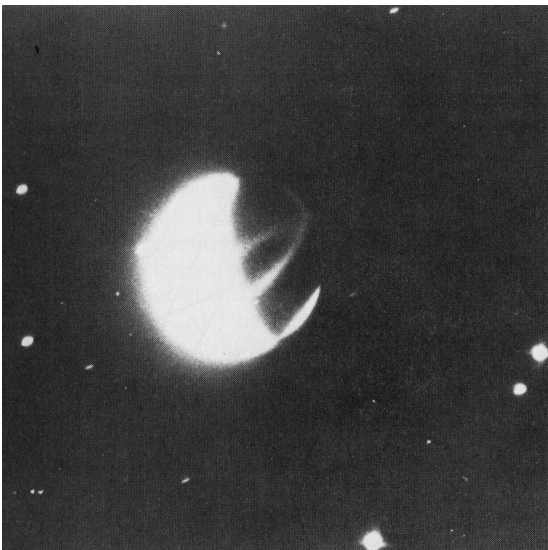


Figure 6: Airglow³

3.2 Aurora Borealis

The Aurora Borealis is a strong luminescence frequently seen in the far northern hemisphere. The responsible physics are gas excitation by incoming solar wind compressed in the earth’s magnetic polar field. Referring to Figure 5 indicates that auroras likely occur near the earth’s poles.

Aurora density is plotted versus altitude in Figure 7 with shadow auroras on the left

and sunlit auroras on the right.⁹ Shadow auroras occur above 80 km with a peak at 100 km. The physics suggests aurora density will scale with free electron density. From Figure 4, free electrons become dominant above 100 km, with a peak near 150 km. Thus, auroras can naturally exist only in the “rarefied” portion of earth’s atmosphere.

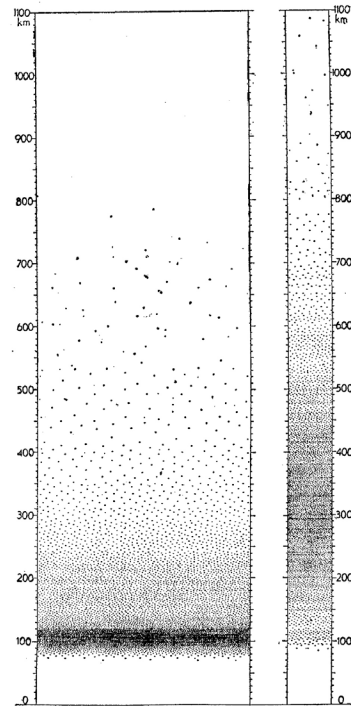


Figure 7: Aurora Density:⁹ Shadow (left) and Sunlit (right)

3.3 Sprites, Elves, and Blue Jets

The newest³ phenomenon are sprites, elves, and blue jets. These *phenomena* are flashes electromagnetically generated by lightning occurring around 100 km and down to thunderstorm clouds¹¹. *Several references state that the conductivity ledge or jump (see Fig. 4) contributes to a rapid reduction in sprite and blue jet formation above 70 km.*^{12;13} In the dense lower atmosphere, electromagnetic discharges form lightning by heating the local air.¹¹ Figure 8 shows the typical structure and altitudes of electromagnetic discharges in the atmosphere.

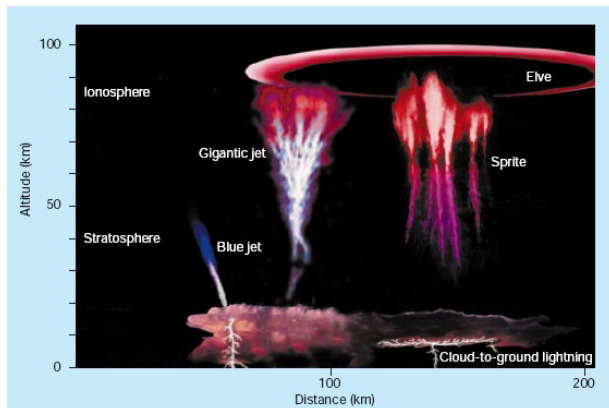


Figure 8: Electromagnetic Discharges in the Atmosphere: Structure and Altitude¹⁴

Sprites appear as red mushrooms above a lightning flash. *Sentman*¹⁵ summarized sprites as: “The brightest region of a unit sprite, its ‘head,’ lies between characteristic

³Interestingly, sprites were accidentally discovered in 1989!¹⁰ Jets were confirmed in 1994.¹⁰

*altitudes of 66 km and 74 km... faint tendrils may extend downward to altitudes of 40–50 km, changing from red near the collar to blue at their lowest extremities.” The upper red color occurs from nitrogen ionization.*¹⁶ The first color photo¹⁵ of a red sprite is given in Figure 9. The Space Shuttle was used for overhead videotaping of sprites after the initial discovery.¹⁰ Sprite formation is approximately 10 milliseconds.¹⁰

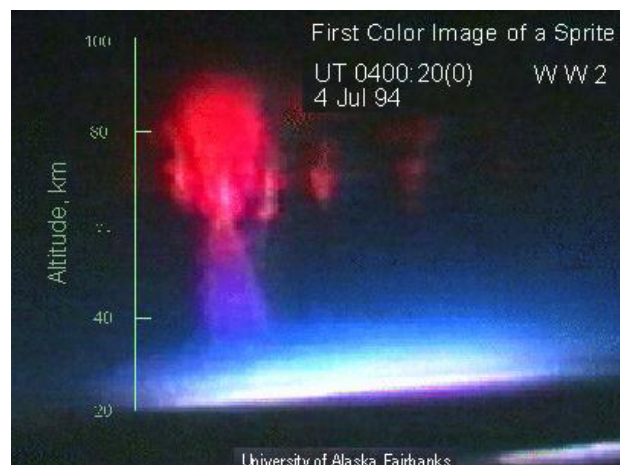


Figure 9: First Color Photo of a Red Sprite by the University of Alaska at Fairbanks¹⁵

Elves appear as circular structures at high altitudes. Interestingly, Boeck says,¹⁰

The one millisecond lifetime of *elves* explains why there have been no eyewitness accounts describing a brief flash that would fill the entire night sky for any observer within a 100 km radius

*Also interesting, Pasco*¹⁴ states that these high altitude discharges “have the ability to

produce highly active chemical species and can effectively ‘treat’ thousands of cubic kilometres of atmosphere.”

Jets are blue columns forming above thunderclouds. Propagation speed¹⁰ (10^5 m/s) is similar to lightning. Figure 10 shows a blue jet photographed by Su.¹² *Su*¹² states, “The trailing jets in all five events assume a conic shape with a $\approx 25^\circ$ conic angle, similar to the turbulence jet emerging from a nozzle.” Again, the rapid rise in conductivity above 70 km effectively reduces jet formation above this altitude.¹²

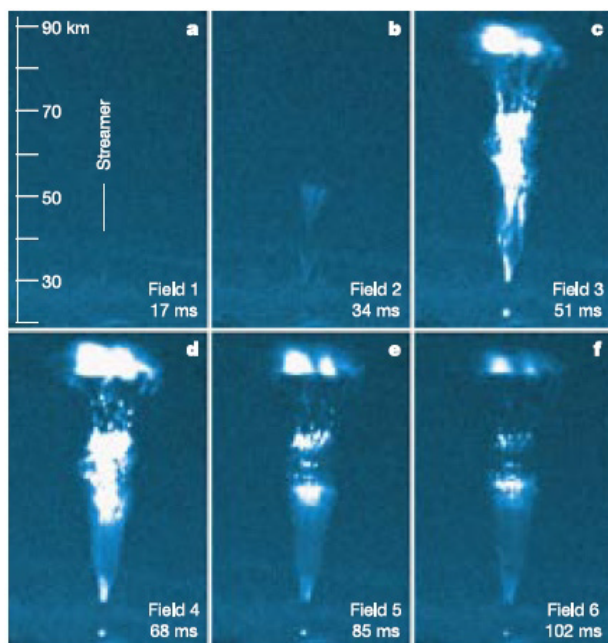


Figure 10: Blue Jet¹²

The physical process of sprite and *elf* generation is not fully understood.^{11;10} Tonev suggests that electromagnetic conductivity in the rarefied atmosphere is critical in sprite formation.¹³

3.4 Cosmic and Interstellar Winds

Beyond the Earth’s, cosmic and interstellar winds provide weak but omnipotent flows. For example, comet tails are streamers in the cosmic wind. Solar wind formation is tightly coupled with solar magnetic fields and corona eruptions.¹⁷ Figure 11 gives a speed map for the solar wind. Solar wind speeds are lowest along the ‘equator’ of the sun and strongest at the poles.

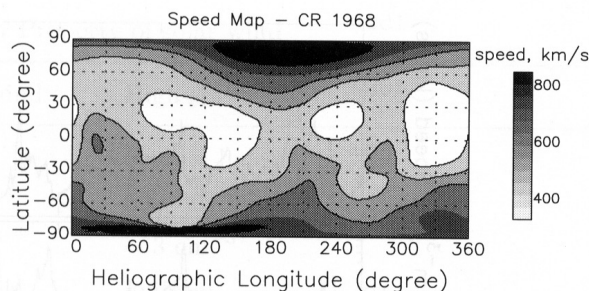


Figure 11: Solar Wind Speed Map¹⁸

The Voyager 1 spacecraft passed the solar wind’s termination shock at 85AU in August 2002.¹⁹ Krimigis says¹⁹ “The outer limit of the Solar System is often considered to be at the distance from the Sun where the solar wind changes from supersonic to subsonic flow.”

4 Aerodynamics

This section discusses rarefied aerodynamics. Muntz presents a historical, theoretical, and computational review of rarefied gas dynamics.²⁰

4.1 Hypersonics

Hypersonic vehicles often encounter rarefied flows because of high operating altitudes and high Mach numbers. This is seen by remembering that *Knudsen* number is,

$$Kn = \sqrt{\frac{\pi\gamma}{2}} \frac{Ma}{Re}$$

Tirsky²¹ presents a regime map for altitude and velocity (Fig. 12). The map shows applicability regions of fluid assumptions such as: equilibrium, perfect gas, frozen flow, etc. The bold curve I indicates the typical path of a spacecraft during re-entry.

Ivanov²² states, “Local rarefied regions can exist, for example, near sharp leading edges of promising winged space vehicles, while the vehicle as a whole is in the continuum regime.” Tai’s²³ results show significant differences between rarefied and continuous Mach distributions for supersonic traditional airfoils. Tai also found that drag increases with increasing altitude regardless of the slip boundary condition.²³

Re-entry vehicles are designed for high drag and thermal dissipation.²⁴ For example, Figure 13 shows the flow field and vehicle geometry for the Mars Microprobe. Notice the shock structure lies almost flat on the nose cone.

Gasdynamics models for hypersonic flow become complex²¹ because dissociation occurs and the flow becomes chemically varying.

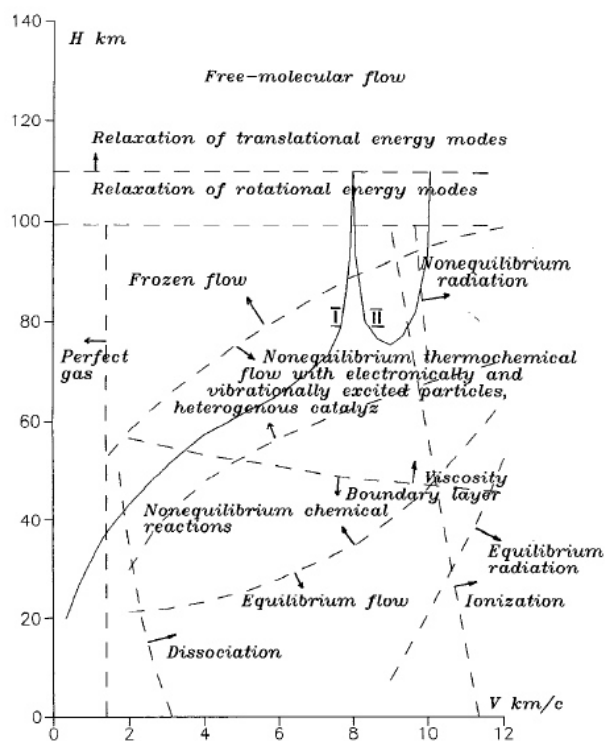


Figure 12: Altitude and Velocity Region Map²¹

4.2 Shuttle

NASA’s Space Shuttle operates across a wide range of Mach, Reynolds and *Knudsen* number flows: continuum and nearly incompressible (220 mph²⁵) for a sea-level landing to free-molecular during orbit (17500 mph at 170 miles²⁵). Figure 14 plots the Shuttle’s entry trajectory with respect to Mach, Reynolds, *Knudsen* Number, and altitude.²⁶ Above 200 km, the regime is free molecular. Between 200 and 105 km, the regime is transition.

According to Blanchard²⁷, “Extensive wind-tunnel testing went into the develop-

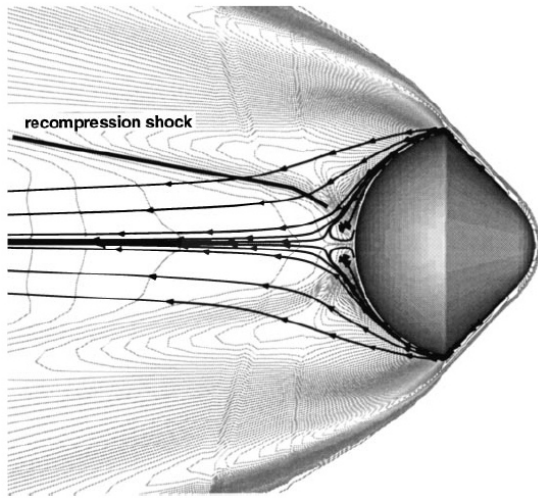


Figure 13: Mars Microprobe Entry Flow (Mach 29)²⁴

ment of the Shuttle Orbiter, but not under the conditions for the rarefied flow regime... prior to the initial Orbiter development flights, no applicable rarefied flow re-entry aerodynamics test data were available.” Shuttle aerodynamic derivatives are currently available from numerous computational²⁶ and experimental^{27;28} sources. The *Knudsen* number effect on the L/D ratio (Fig. 15) shows the Shuttle’s known aerodynamics in the “early 1980’s.”²⁷ The lift to drag ratio decreases as Kn increases. The Shuttle’s pitch moment changes with Kn (Fig. 16). The figure compares the pitch moment with experiments and computations. The lack of wind-tunnel data above an effective 100 km altitude is apparent.

The Columbia re-entry —doomed by a hole in the Shuttle’s leading edge— subtly illustrates how the hot but rarefied air dur-

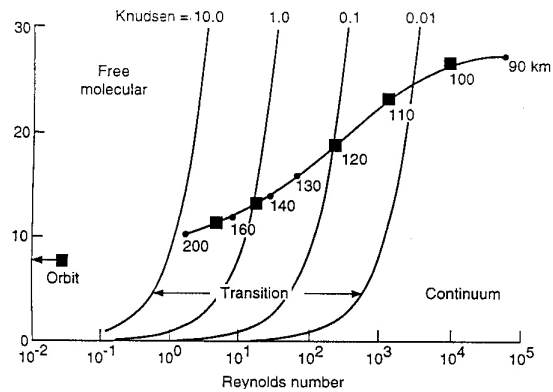


Figure 14: Shuttle Trajectory²⁶

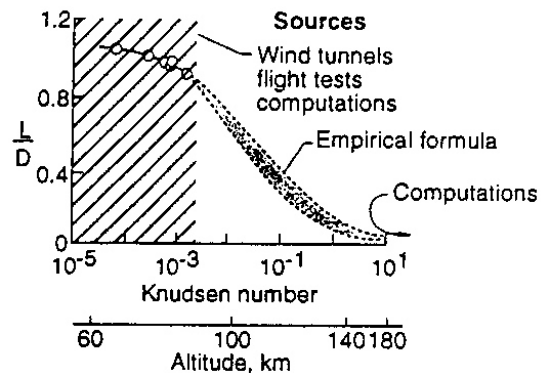


Figure 15: Shuttle Lift/Drag²⁶

ing re-entry stretched the failure time when compared *with* lower atmospheric failures. From the Columbia Accident Investigation Report²⁵, the shuttle entered the “effective” atmosphere at 120km. The first recorded problem is at 270 seconds just under 100 km. Effective structural failure occurred 922 seconds after entry at 61 km. Figure 17 shows the flow velocities through the leading-edge hole. The report estimated the leading edge air temperature to be 5000 F.

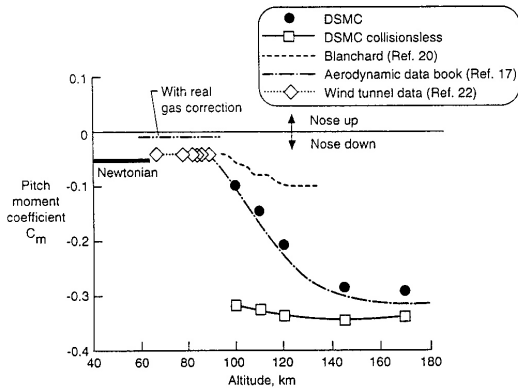


Figure 16: Shuttle Pitch Moment²⁷

4.3 Satellites

Satellites —and especially Low Earth Orbit (LEO) Satellites— experience orbit degradation caused by rarefied aerodynamics. Haas²⁹ found with a DSMC simulation that the Magellan spacecraft’s roll moment coefficients in rarefied flows were twice as large as the free-molecular coefficients. Harrison calculates LEO drag with a free-molecular method and known orbits of multiple satellites.³⁰ In particular, the particle reflections were found to be “low velocities, in a near specular direction.” Figure 18 shows a comparison of the lift and drag coefficients for a flat plate with respect to helium and oxygen.

Interestingly, Cho³¹ proposes orbital debris removal using laser induced propulsion. Cho claims that small debris (1 cm–10 cm) is common and dangerous in LEO. The proposal requires a laser equipped satellite to detect, track and hit a particular debris item. Figure 19 shows the removal time required versus debris mass.

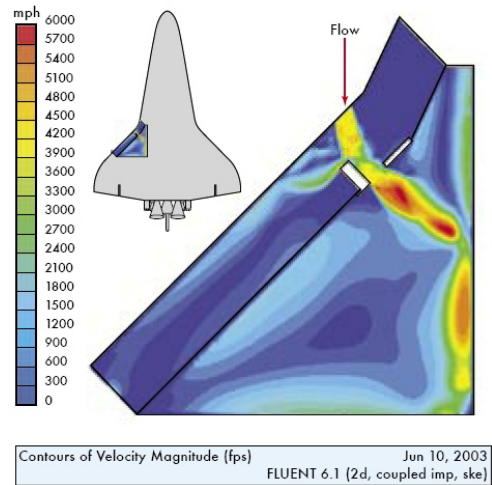


Figure 17: Columbia Damage Flow²⁵

5 Conclusions

Rarefied upper atmosphere flows are complicated but allow for interesting phenomena. Flows at high altitudes behave counter to intuition mainly because of rarefied *Knudsen* effects and especially electromagnetic influences. Atmospheric meteorology continues past the troposphere’s convective dominated region. Rarefied gas dynamics allows for interesting natural *phenomena* in the upper atmosphere. Future research should likely focus on experimental measurements of the upper atmosphere, especially with respect to electromagnetics and ionization.

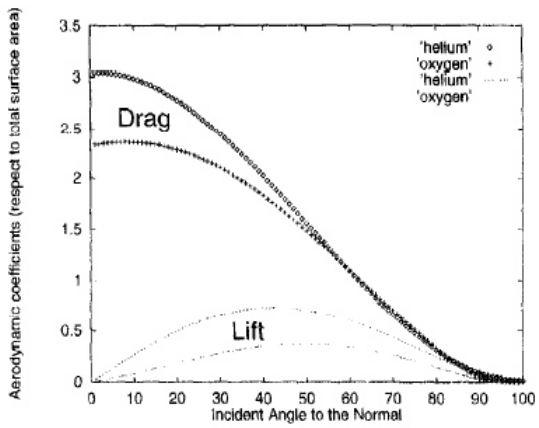


Figure 18: Rarefied Flow Flat Plate Drag³⁰

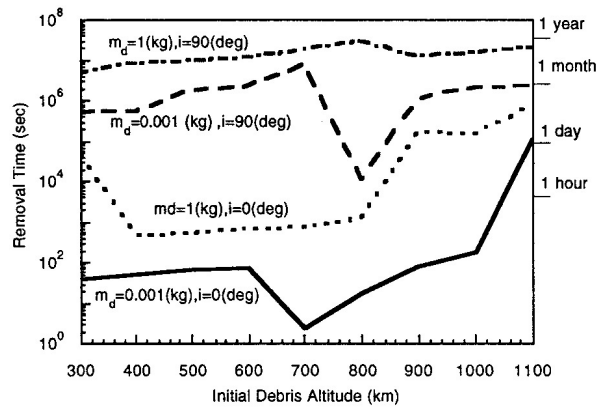


Figure 19: Debris Removal Time³¹

References

- [1] Dowling, T. E., “Dynamics of Jovian Atmospheres,” *Annu. Rev. Fluid Mech.*, Vol. 27, 1995, pp. 293–334.
- [2] *Guide to reference and standard atmosphere models*, American Institute of Aeronautics and Astronautics, 1997.
- [3] *The Upper Atmosphere and Magnetosphere*, National Academy of Sciences, Washington, D.C., 1977.
- [4] Wallace, J. M., *Atmospheric Science*, Academic Press, Inc., New York, 1st ed., 1977.
- [5] Doswell, C. A., editor, *Severe Convective Storms*, Vol. 28, American Meteorological Society, Boston, MA, November 2001.
- [6] Siingh, D., Singh, R. P., Kamra, A. K., Gupta, P. N., Singh, R., Gopalakrishnan, V., and Singh, A. K., “Review of electromagnetic coupling between the Earth’s atmosphere and the space environment,” *Journal of Atmospheric and Solar-Terrestrial Physics*, Vol. 67, 2005, pp. 637–658.
- [7] Ratcliffe, J. A., *Physics of the Upper Atmosphere*, Academic Press, New York, 1st ed., 1960.
- [8] Smith, S. M., Friedman, J., Raizada, S., Tepley, C., Baumgardner, J., and Mendillo, M., “Evidence of mesospheric bore formation from a breaking gravity wave event: simultaneous imaging and lidar measurements,” *Journal of Atmospheric and Solar-Terrestrial Physics*, Vol. 67, 2005, pp. 345–356.
- [9] Rawer, K., *The Ionosphere*, Frederick Ungar Publishing Co., New York, 1st ed., 1952.
- [10] Boeck, W., Vaughan, O. H., Blakeslee, R. J., Vonnegut, B., and Brook, M., “The role of the space shuttle videotapes in the discovery of sprites, jets and elves.” *Journal of Atmospheric and Solar-Terrestrial Physics*, Vol. 60, 1998, pp. 669–677.
- [11] Bering, E. A., Benbrook, J. R., Garrett, J. A., Paredes, A. M., Wescott, E. M., Moudry, D. R., Sentman, D. D., Stenbaek-Nielsen, H. C., and Lyons, W. A., “Sprite and Elve Electrodynamics,” *Adv. Space Res.*, Vol. 30, No. 11, 2002, pp. 2585–2595.
- [12] Su, H. T., Hsu, R. R., Chen, A. B., Wang, Y. C., Hsiao, W. S., Lai, W. C., Lee, L. C., Sato, M., and Fukunishi, H., “Gigantic jets between a thundercloud and the ionosphere,” *Nature*, Vol. 423, June 2003.
- [13] Tonev, P. T. and Velinov, P. I. Y., “Modelling the influence of conductivity profiles on red sprite formation and structure,” *Advances in Space Research*, Vol. 34, 2004, pp. 1792–1797.
- [14] Pasko, V. P., “Atmospheric physics: Electric jets,” *Nature*, Vol. 423, 26 June 2003, pp. 927–929.

- [15] Sentman, D. D., Wescott, E. M., Osborne, D. L., Hampton, D. L., and Heavner, M. J., “Preliminary results from the Sprites94 aircraft campaign: 1. Red sprites,” *Geophysical Research Letters*, Vol. 22, No. 10, May 1995, pp. 1205–1208.
- [16] Hampton, D. L., Heavner, M. J., Wescott, E. M., and Sentman, D. D., “Optical spectral characteristics of sprites,” *Geophys. Res. Lett.*, Vol. 23, No. 1, 1996, pp. 89–92.
- [17] Jokipii, J. R., Sonett, C. P., and Giampapa, M. S., editors, *Cosmic Winds and the Heliosphere*, The University of Arizona Press, Tucson, 1st ed., 1997.
- [18] Antia, H. M., Bhatnagar, A., and Ulmschneider, P., editors, *Lectures on Solar Physics*, Springer, Heidelberg, 1st ed., 2003.
- [19] Krimigis, S. M., Decker, R. B., Hill, M. E., Armstrong, T. P., Gloeckler, G., Hamilton, D. C., Lanzerotti, L. J., and Roelof, E. C., “Voyager 1 exited the solar wind at a distance of 85 AU from the Sun,” *Nature*, Vol. 426, No. 6, Nov 2003, pp. 45–48.
- [20] Muntz, E. P., “Rarefied Gas Dynamics,” *Ann. Rev. Fluid Mech.*, Vol. 21, 1989, pp. 387–417.
- [21] Tirsky, G. A., “Up-To-Date Gasdynamic Models of Hypersonic Aerodynamics and Heat Transfer with Real Gas Properties,” *Annu. Rev. Fluid Mech.*, Vol. 25, 1993, pp. 151–181.
- [22] Ivanov, M. S. and Gimelshein, S. F., “Computational Hypersonic Rarefied Flows,” *Annu. Rev. Fluid Mech.*, Vol. 30, 1998, pp. 469–505.
- [23] Tai, T. C. and Moran, M. S., “Supersonic Low-Density Flow Over Airfoils,” *Journal of Aircraft*, Vol. 26, No. 12, 1989, pp. 1118–1122.
- [24] Gnoffo, P. A., “Planetary-Entry Gas Dynamics,” *Annu. Rev. Fluid Mech.*, Vol. 31, 1999, pp. 459–494.
- [25] “Columbia Accident Investigation Board,” Tech. rep., NASA, Washington, D.C., August 2003.
- [26] Rault, D. F. G., “Aerodynamics of the Shuttle Orbiter at High Altitudes,” *Journal of Spacecraft and Rockets*, Vol. 31, No. 6, 1994, pp. 944–952.
- [27] Blanchard, R. C., Larman, K. T., and Moats, C. D., “Rarefied-Flow Shuttle Aerodynamics Flight Model,” *Journal of Spacecraft and Rockets*, Vol. 31, No. 4, July–August 1994, pp. 550–556.
- [28] Blanchard, R. C. and Buck, G. M., “Determination of rarefied-flow aerodynamics of the shuttle orbiter from flight measurements on STS-6 and STS-7,” AIAA Paper 85-0347, 1985.
- [29] Haas, B. L. and Schmitt, D. A., “Simulated Rarefied Aerodynamics of the

Magellan Spacecraft During Aerobraking,” *Journal of Spacecraft and Rockets*, Vol. 31, No. 6, November–December 1994, pp. 980–985.

- [30] Harrison, I. K. and Swinderd, G. G., “A free molecule aerodynamic investigation using multiple satellite analysis,” *Planet. Space Sci.*, Vol. 44, No. 2, 1996, pp. 171–180.
- [31] Cho, M., “Removal of Orbital Debris from Low Earth Orbit by Laser-Generating Drag,” *Journal of Spacecraft and Rockets*, Vol. 31, No. 5, 1993, pp. 920–922.